Supporting information for

Large-cavity coronoids with different inner and outer edge structures

Marco Di Giovannantonio,[1,*,‡] Xuelin Yao,[2,‡] Kristjan Eimre,[1,‡] José I. Urgel,[1] Pascal Ruffieux,[1] Carlo A. Pignedoli,[1,*] Klaus Müllen,[2,3,*] Roman Fasel,[1,5] Akimitsu Narita[2,4,*]

[1]*Empa, Swiss Federal Laboratories for Materials Science and Technology, nanotech@surfaces Laboratory, 8600 Dübendorf, Switzerland*
[2]*Max Planck Institute for Polymer Research, 55128 Mainz, Germany*
[3]*Institute of Physical Chemistry, Johannes Gutenberg University Mainz, Duesbergweg 10-14, 55128 Mainz, Germany*
[4]*Organic and Carbon Nanomaterials Unit, Okinawa Institute of Science and Technology Graduate University, Okinawa 904-0495, Japan*
[5]*Department of Chemistry and Biochemistry, University of Bern, 3012 Bern, Switzerland*
[#]*These authors contributed equally*

Table of Contents

1. **Methods**
2. **Precursor synthesis and characterizations**
3. **Additional experimental and computational results**

1. Methods

STM/STS and nc-AFM experiments.
The on-surface synthesis experiments were performed under ultrahigh vacuum (UHV) conditions with base pressure below 2×10^{-10} mbar. Au(111) substrates (MaTeck GmbH) were cleaned by repeated cycles of Ar^+ sputtering (1 keV) and annealing (460 ºC). The precursor molecules were thermally evaporated onto the clean Au(111) surface from quartz crucible heated at a temperature ranging from 130 to 175 ºC, resulting in a deposition rate ranging from 0.23 to 2.85 monolayer/hour (ML/h). STM images were acquired with a low-temperature scanning tunneling microscope (Scienta Omicron) operated at 5 K in constant-current mode using an etched tungsten tip. Bias voltages are given with respect to the sample. Constant-height dI/dV spectra and maps were obtained with a lock-in amplifier (f = 610 Hz). Nc-AFM measurements were performed at 5 K with a tungsten tip placed on a QPlus tuning fork sensor.[1] The tip was functionalized with a single CO molecule at the tip apex picked up from the previously CO-dosed surface.[2] The sensor was driven at its resonance frequency (27050 Hz) with a constant amplitude of 70 pm. The frequency shift from resonance of the tuning fork was recorded in constant-height mode using Omicron Matrix electronics and HF2Li PLL by Zurich Instruments. The Δz is positive (negative) when the tip-surface distance is increased (decreased) with respect to the STM setpoint at which the feedback loop is open.

Computational details.
The DFT calculations on Au(111) surfaces were performed with the CP2K code[3] utilizing the AiiDA platform.[4] The electronic states were expanded with a TZV2P Gaussian basis set[5] for C and H species and a DZVP basis set for Au species. A cutoff of 600 Ry was used for the plane wave basis set. We used Norm Conserving Goedecker-Teter-Hutter[6] pseudopotentials and the PBE[7] exchange-correlation functional with the D3 dispersion corrections proposed by Grimme.[8] The surface/adsorbate systems were modelled within the repeated slab scheme, i.e. a simulation cell containing 4 atomic layers of Au along the [111] direction and a layer of hydrogen atoms to passivate one side of the slab in order to suppress one of the two Au(111) surface states. 40 Å of vacuum were included in the simulation cell to decouple the system from its periodic replicas in the direction perpendicular to the surface. We considered supercells of 41.27 x 40.85 Å corresponding to 224 surface units. To obtain the equilibrium geometries we kept the atomic positions of the bottom two layers of the slab fixed to the ideal bulk positions, all other atoms were relaxed until forces were lower than 0.005 eV/Å. To obtain simulated STM images within the Tersoff-Hamann approximation,[9] we extrapolated the electronic orbitals obtained from CP2K to the vacuum region in order to correct the wrong decay in vacuum of the charge density due to the localized basis.

The ProbeParticle model[10] was used to simulate nc-AFM images. We used a 2-point implementation of the model where two probe particles represent the carbon and oxygen atoms in the CO molecule. The stiffness parameters of the ProbeParticle as well as the Lennard-Jones parameters of the tip were obtained by fitting to DFT calculations for an isolated PTCDA molecule and an isolated pentacene molecule.[11] The charges of the tip atoms were assigned by the restrained electrostatic potential method[12] applied in the case of the pentacene molecule. For the tip sample electrostatic interactions the Hartree potential obtained from the CP2K calculations was used.

The gas-phase electronic structure and local aromaticity calculations were performed with the Gaussian 09 D.01 code[13] at the UB3LYP/6-311+G** // UB3LYP/6-311G** level of theory. The $NICS_{zz}(1)$[14] was calculated with the GIAO-UB3LYP/6-311+G** method as the magnetic shielding tensor component perpendicular to each local carbon cycle evaluated at height 1 Å away from the center (average of the above and below value). The anisotropy of the induced current density (ACID) calculations[15,16] were performed with the CSGT method.[17]

HOMA analysis was performed based on the UB3LYP/6-311G** geometries. The method was calibrated such that the HOMA value of 1.0 corresponds to benzene and 0.0 corresponds to a hypothetical cyclic non-aromatic system with alternating double and single bonds, with double and single bond lengths calculated from butadiene.

2. Precursor synthesis and characterizations

All commercially available chemicals were used without further purification unless otherwise noted. Column chromatography was done with silica gel (grain size of 0.04–0.063 mm) and thin layer chromatography (TLC) was performed on silica gel-coated aluminum sheets with F254 indicator. Nuclear Magnetic Resonance (NMR) spectra were recorded on AVANCE 300 MHz, AVANCE 500 MHz or 700 MHz Bruker spectrometers. Chemical shifts were reported in ppm. Coupling constants (*J* values) were reported in Hertz. ^{1}H NMR chemical shifts were referenced to CD_2Cl_2 (5.320 ppm) or $C_2D_2Cl_4$ (6.000 ppm). ^{13}C NMR chemical shifts were referenced to CD_2Cl_2 (54.00 ppm) or $C_2D_2Cl_4$ (73.78 ppm). Abbreviations: s = singlet, d = doublet, t = triplet, m = multiplet). High-resolution mass spectroscopy (HRMS) was performed on a SYNAPT G2 Si high resolution time-of-flight mass spectrometer (Waters Corp., Manchester, UK) by matrix-assisted laser deposition/ionization (MALDI). Melting points were measured with a Büchi B-545 apparatus. 1,3-Dibromo-2-iodobenzene (**2**) was synthesized according to a reported procedure.[18] 4,4,5,5-Tetramethyl-2-{2-[(triisopropylsilyl)ethynyl]phenyl}-1,3,2-dioxaborolane (**4**) was prepared following a reported procedure.[19]

Synthetic route towards precursor 1[a]

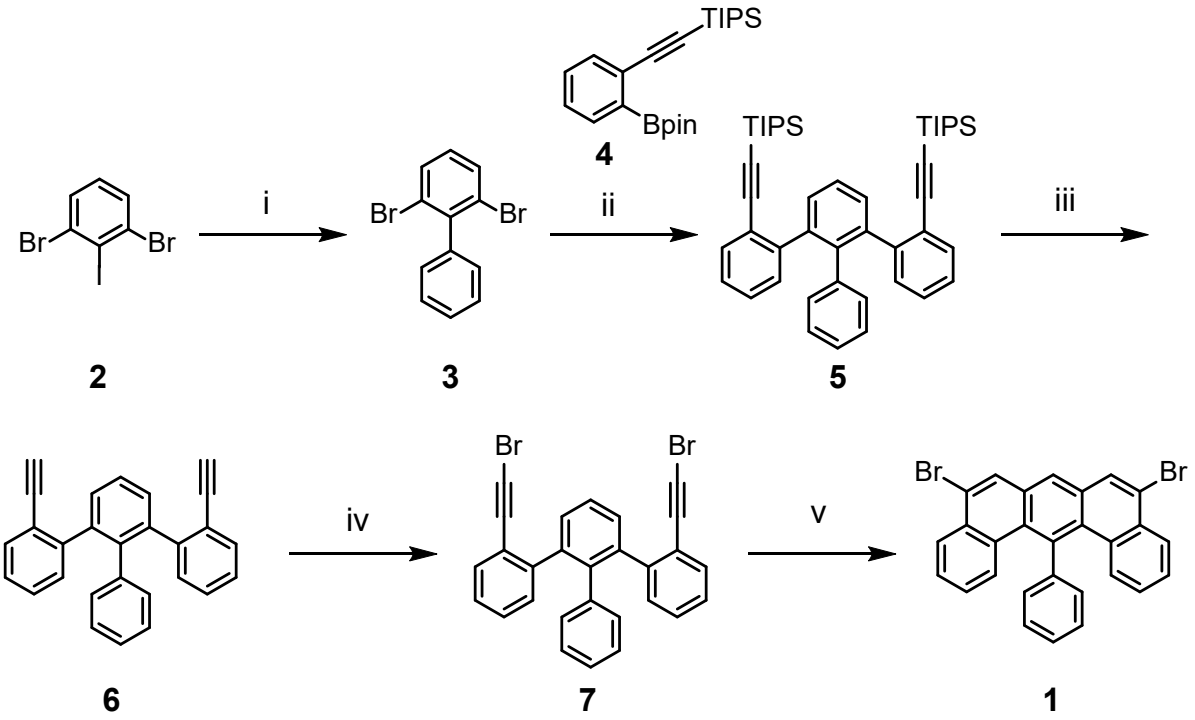

[a]Reagents and conditions: (i) phenylboronic acid, $NaHCO_3$, $PdCl_2(dppf)\cdot CH_2Cl_2$, DMSO/$H_2O$, 55 ºC, 72 h, 48%; (ii) K_2CO_3, $Pd(PPh_3)_4$, dioxane/ethanol/H_2O, 100 ºC, 12 h, 89%; (iii) TBAF, THF, r.t., 12 h, 98%; (iv) *N*-bromosuccinimide, $AgNO_3$, acetone, r.t., 3 h, 82%; (v)

AuCl, toluene, 60 ºC, 24 h, 57%. TIPS: triisopropylsilyl. Bpin: pinacol boronate. dppf: 1,1'-bis(diphenylphosphino)ferrocene. DMSO: dimethyl sulfoxide. THF: tetrahydrofuran.

For the synthesis of [6]coronoid we have designed the U-shaped precursor **1**, 5,9-dibromo-14-phenylbenzo[*m*]tetraphene, having a benzo[*m*]tetraphene core with a pre-installed zigzag edge as well as two bromo groups carefully positioned to allow for the macrocyclization on surface. Towards the synthesis of precursor **1**, bis(triisopropylsilylethynyl)-substituted oligophenyl **5** was initially prepared via selective Suzuki-Miyaura coupling of 1,3-dibromo-2-iodobenzene (**2**) with phenylboronic acid, followed by twofold Suzuki-Miyaura coupling with boronic ester **4**. Deprotection of **5** with tetrabutylammonium fluoride (TBAF) and subsequent bromination of the ethynyl groups of **6** gave bis(bromoethynyl)-substituted oligophenyl **7**. Finally, gold-catalyzed cyclization of **7** afforded the U-shaped precursor **1**.

Synthesis of 2,6-Dibromo-1,1'-biphenyl (3)

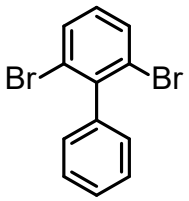

2,6-Dibromoiodobenzene (**2**) (5.00 g, 13.8 mmol) and phenylboronic acid (2.02 g, 16.7 mmol) were dissolved in 60 mL of dimethyl sulfoxide in a 250-mL round-bottom flask. A solution of sodium hydrogen carbonate (3.48 g, 41.5 mmol) in 10 mL water was added and the resulting suspension was bubbled with argon for 1 h. 1,1'-Bis(diphenylphosphino)ferrocene-palladium(II)dichloride dichloromethane complex (564 mg, 0.691 mmol) was subsequently added followed by further degassing with argon for 20 min. The reaction mixture was heated to 55 °C for 72 h. After addition of water (100 mL), the mixture was extracted with dichloromethane (three times), washed with water and the organic phase was dried over magnesium sulfate. After removal of solvent under reduced pressure, the residue was purified via column chromatography over silica gel using hexane as eluent to afford compound **3** as white solid (2.06 g, 48% yield). Melting point: 72.1 – 73.4 °C. ^{1}H NMR (300 MHz, CD_2Cl_2, 298 K, ppm) δ 7.66 (d, J = 8.0 Hz, 2H), 7.52 – 7.40 (m, 3H), 7.22 (d, J = 6.2 Hz, 2H), 7.10 (t, J = 8.0 Hz, 1H). ^{13}C NMR (75 MHz, CD_2Cl_2, 298 K, ppm) δ 143.32, 141.64, 132.28, 130.38, 129.59, 128.60, 128.47, 124.81. HRMS (MALDI-TOF, positive) *m/z*: Calcd for $C_{12}H_8Br_2$: 309.8993; Found: 309.8974 $[M]^+$.

Synthesis of 2-triisopropylsilylethynyl-3'-(2-triisopropylsilylethynylphenyl)-1,1':2',1''-terphenyl (5)

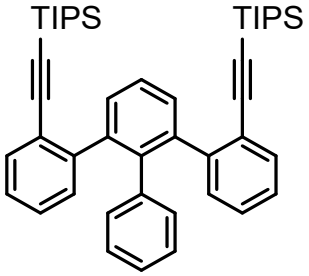

2,6-Dibromo-1,1'-biphenyl (**3**) (0.500 mg, 1.60 mmol) and 4,4,5,5-tetramethyl-2-{2-[(triisopropylsilyl)ethynyl]phenyl}-1,3,2-dioxaborolane (**4**) (1.85 g, 4.80 mmol) were dissolved in 20 mL of dioxane, then aqueous potassium carbonate (2 M, 4.8 mL) and ethanol (4.8 mL) were added. The resulting mixture was subjected to freeze-pump-thaw (three cycles) and tetrakis(triphenylphosphine)palladium(0) (0.290 g, 0.200 mmol) was added. The resulting mixture was stirred at 100 °C for 12 h. After cooling to room temperature, water was added. The mixture was extracted with dichloromethane, washed with brine, dried over magnesium sulfate and concentrated in vacuo. The residue was purified by column chromatography over silica gel with hexane as eluent to provide **5** as a slightly yellow oil (956 mg, 89% yield). ^{1}H NMR (300 MHz, CD_2Cl_2, 298 K, ppm) δ 7.47 (d, J = 7.7 Hz, 2H), 7.36 (s, 3H), 7.14 – 6.86 (m, 9H), 6.74 (d, J = 7.7 Hz, 2H), 1.02 (s, 42H). ^{13}C NMR (75 MHz, CD_2Cl_2, 298 K, ppm) δ 145.79, 140.87, 140.31, 139.75, 132.33, 130.77, 130.55, 127.59, 127.21, 126.65, 126.56, 126.14, 123.93, 106.97, 94.59, 18.80, 11.67. HRMS (MALDI-TOF, positive) *m/z*: Calcd for $C_{46}H_{58}Si_2$: 666.4077; Found: 666.4079 $[M]^+$.

Synthesis of 2-ethynyl-3'-(2-ethynylphenyl)-1,1':2',1''-terphenyl (6)

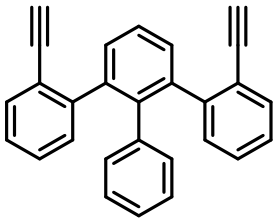

2-Triisopropylsilylethynyl-3'-(2-triisopropylsilylethynylphenyl)-1,1':2',1''-terphenyl (**5**) (956 mg, 1.43 mmol) was dissolved in 60 mL of tetrahydrofuran. The solution was bubbled with argon for 15 min and a 1 M solution of tetra-*n*-butylammonium fluoride in tetrahydrofuran (5.7 mL, 5.7 mmol) was added via syringe. The reaction mixture was stirred at room temperature for 12 h and quenched with water. After extraction with dichloromethane (three times), the organic phases were washed with water and dried over magnesium sulfate and then evaporated to dryness. The residue was purified by column chromatography over silica gel with hexane/dichloromethane (V/V = 5 : 1) as eluent to obtain the title compound as white solid (498 mg, 98% yield). Melting point: 201.3 – 201.7 °C. ^{1}H NMR (300 MHz, CD_2Cl_2, 298 K, ppm) δ 7.55 – 7.31 (m, 5H), 7.21 – 6.82 (m, 11H), 6.91 (s, 2H). ^{13}C NMR (75 MHz, CD_2Cl_2, 298 K, ppm) δ 145.37, 140.72, 139.70, 132.88, 131.43, 131.11, 130.28, 128.20, 127.07, 126.90, 126.53, 126.23, 122.29, 83.46, 80.69. MS (MALDI-TOF, positive) *m/z*: Calcd for $C_{28}H_{18}$: 354.14; Found: 354.15 $[M]^+$.

Synthesis of 2-bromoethynyl-3'-(2-bromoethynylphenyl)-1,1':2',1''-terphenyl (7)

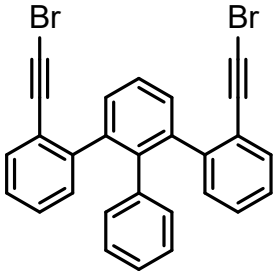

Silver nitrate (23.4 mg, 0.138 mmol) was added to a solution of 2-ethynyl-3'-(2-ethynylphenyl)-1,1':2',1"-terphenyl (**6**) (244 mg, 0.688 mmol) in 40 mL of acetone. Then *N*-bromosuccinimide (368 mg, 2.07 mmol) was added in portions. The mixture was stirred for 3 h at room temperature, and then the resulting mixture was filtrated. The filtrate was extracted with dichloromethane (three times). The combined organic layers were washed with water, dried over magnesium sulfate, and then concentrated in vacuo. The residue was purified by column chromatography over silica gel with hexane/dichloromethane (V/V = 5 : 1) as eluent to afford the titled compound as white solid (289 mg, 82%). Melting point: 66.9 – 67.6 °C. ^{1}H NMR (300 MHz, CD_2Cl_2, 298 K, ppm) δ 7.54 – 7.28 (m, 5H), 7.23 – 7.00 (m, 6H), 6.98 – 6.77 (m, 5H). ^{13}C NMR (75 MHz, CD_2Cl_2, 298 K, ppm) δ 145.54, 140.66, 140.55, 139.51, 132.60, 131.64, 131.13, 130.43, 128.22, 126.95, 126.86, 126.71, 126.21, 122.77, 79.93, 30.11. MS (MALDI-TOF, positive) *m/z*: Calcd for $C_{28}H_{16}Br_2$: 509.96; Found: 509.97 $[M]^+$.

Synthesis of 5,9-dibromo-14-phenylbenzo[*m*]tetraphene (1)

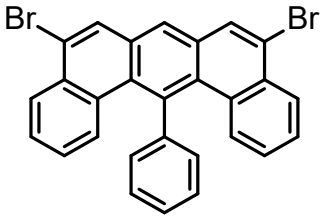

2-Bromoethynyl-3'-(2-bromoethynylphenyl)-1,1':2',1"-terphenyl (**7**) (200 mg, 0.390 mmol) was dissolved in 20 mL of anhydrous toluene. After degassing for 20 min by argon bubbling, gold (I) chloride (37.2 mg, 0.160 mmol) was added. The mixture was stirred at 60 °C for 24 h. After cooling to room temperature, the mixture was filtrated and the filtrate was extracted with dichloromethane (three times). The combined organic layers were washed with water and dried over magnesium sulfate. After removal of the solvent under reduced pressure, the residue was purified by column chromatography over silica gel with hexane as eluent to give precursor **1** as greenish-yellow solid (115 mg, 57%). For the on-surface experiments, precursor **1** was further purified by recrystallization through slow diffusion of methanol into a solution of **1** in chloroform. Melting point: 259.3 – 260.8 °C. ^{1}H NMR (700 MHz, $C_2D_2Cl_4$, 298 K, ppm) δ 8.38 (d, J = 8.1 Hz, 2H), 8.22 (s, 2H), 8.18 (s, 1H), 7.69 (t, J = 7.4 Hz, 1H), 7.65 (t, J = 7.5 Hz, 2H), 7.53 (t, J = 7.5 Hz, 2H), 7.50 (d, J = 7.0 Hz, 2H), 7.40 (d, J = 8.7 Hz, 2H), 7.09 (t, J = 7.7 Hz, 2H). ^{13}C NMR (75 MHz, $C_2D_2Cl_4$, 298 K, ppm) δ 144.06, 138.88, 132.00, 131.73, 131.46, 130.91, 130.73, 130.19, 129.09, 128.37, 127.69, 127.47, 126.90, 125.67, 125.29, 122.95. HRMS (MALDI-TOF, positive) *m/z*: Calcd for $C_{28}H_{16}Br_2$: 509.9619; Found: 509.9615 $[M]^+$.

3. Additional experimental and computational results

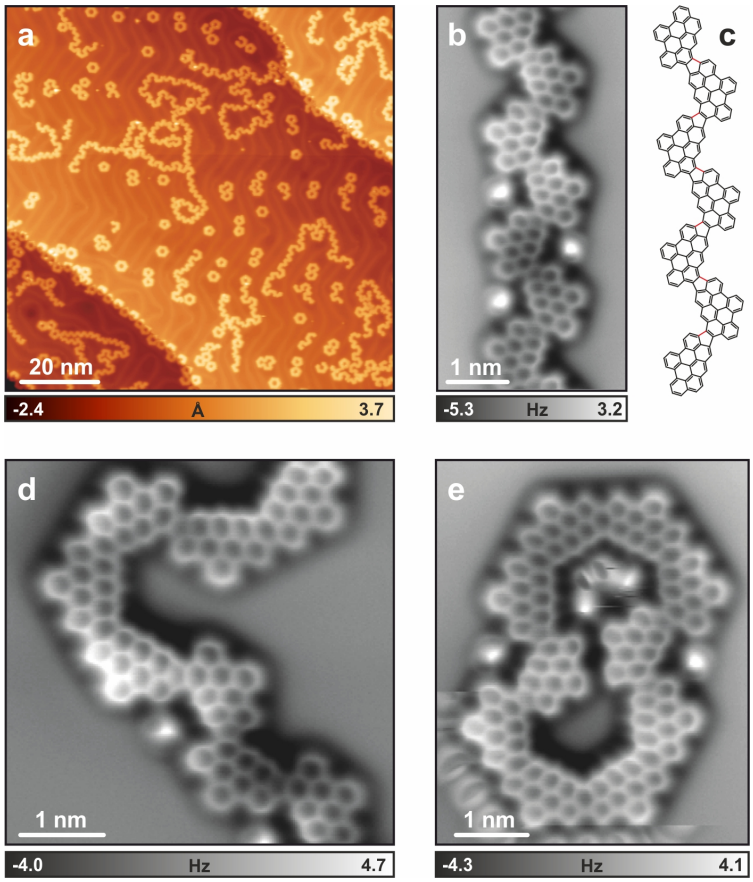

Figure S1. Overview of various structures. (a) Large-scale STM image after deposition of **1** on Au(111) held at 200 °C and subsequently annealed to 380 °C. (b,d,e) nc-AFM images of different segments showing that the precursor molecules can couple to each other in two different configurations, *cis* and *trans*, giving rise to complex, randomly oriented chains and closed loops. *Cis* connections between precursors **1** lead, after cyclodehydrogenation, to all-benzenoid segments, while *trans* connections give rise to the formation of five-membered rings, as highlighted by the red bonds in panel (c). If only *cis* connections are present, [5]- and [6]coronoids are formed (see main text). No larger coronoids (e.g. [7]coronoid) have been observed. The bright point-like features observed in panel b,d,e are CO molecules co-adsorbed on the Au(111) surface for tip functionalization. Scanning parameters: (a) V_b = –0.5 V, I_t = 50 pA; (b) Δz = +2.32 Å with respect to STM set point: –5 mV, 100 pA; (d) Δz = +2.67 Å with respect to STM set point: –5 mV, 100 pA; (e) Δz = +2.64 Å with respect to STM set point: –5 mV, 100 pA.

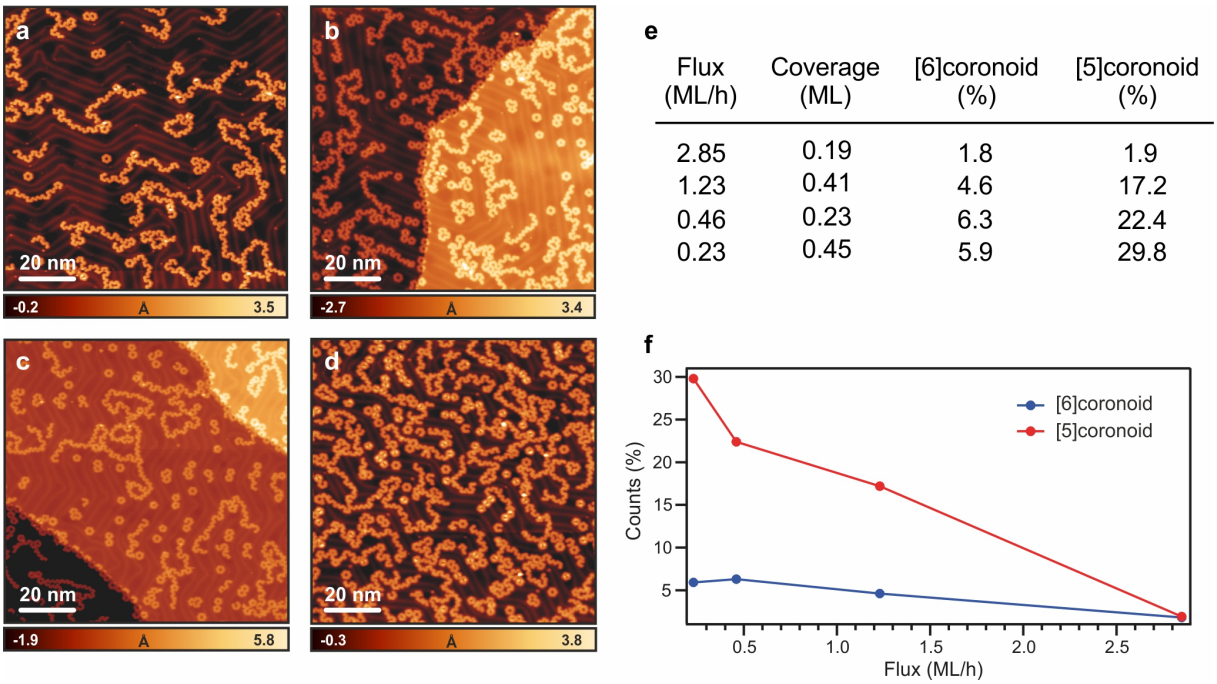

e

Flux (ML/h)	Coverage (ML)	[6]coronoid (%)	[5]coronoid (%)
2.85	0.19	1.8	1.9
1.23	0.41	4.6	17.2
0.46	0.23	6.3	22.4
0.23	0.45	5.9	29.8

Figure S2. Yield of coronoids as a function of precursor deposition flux. (a-d) STM images after deposition of **1** on the Au(111) surface held at 200 °C and subsequent annealing to 380 °C. Different deposition flux of the precursor molecules is used in the four cases, as reported in the table of panel (e), together with the corresponding coverages (from top to bottom, from (a) to (d), respectively). The number of monomers forming [6]- and [5]coronoids (in percentage) is indicated in the table and plotted in the graph of panel (f). Scanning parameters: (a) $V_b = -1$ V, $I_t = 100$ pA; (b) $V_b = -0.7$ V, $I_t = 100$ pA; (c) $V_b = -0.5$ V, $I_t = 50$ pA; (d) $V_b = -1$ V, $I_t = 30$ pA. The relative abundance of monomers forming specific structures has been determined from several 100×100 nm^2 STM images, counting 2344, 1165, 3257 and 2333 monomers for the cases (a), (b), (c) and (d), respectively.

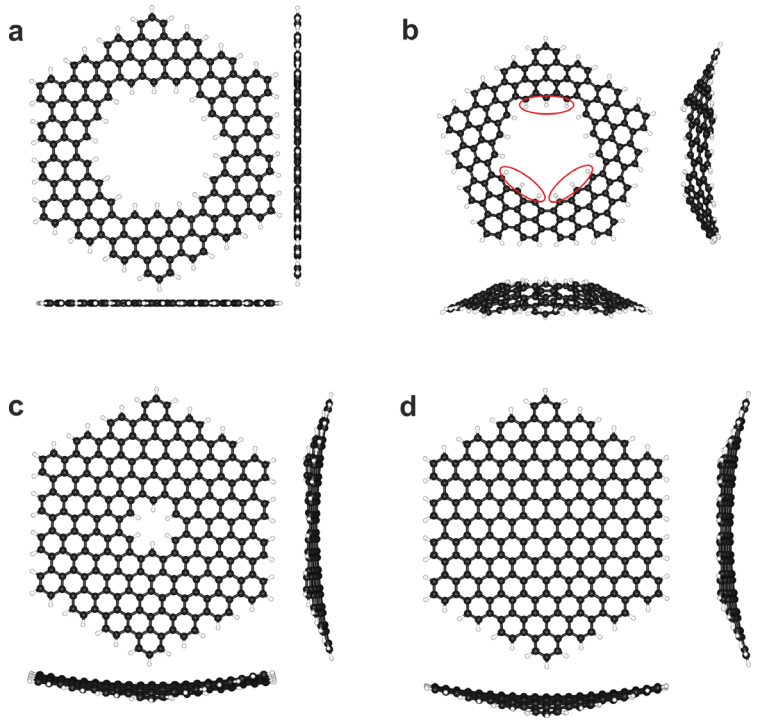

Figure S3. Gas phase optimized geometries. Front and side views of the [6]coronoid **C168** (a), [5]coronoid **C140** (b), **C216** (c), and **C222** (d). Red ellipses in panel b indicate slightly raised hydrogens due to steric hindrance with neighboring zigzag segments. All optimizations were performed at the B3LYP/6-311G** level of theory. The pore size of the [6]coronoid **C168** (1.45 nm) and of **C216** (0.58 nm) are defined as the C-C distance between the central carbon atoms of two opposing inner edges. The pore size of the [5]coronoid **C140** (1.17 nm) is defined as the diameter of the circle inscribed into the pore projection and crossing the central carbon atoms of the zigzag edges closest to the center.

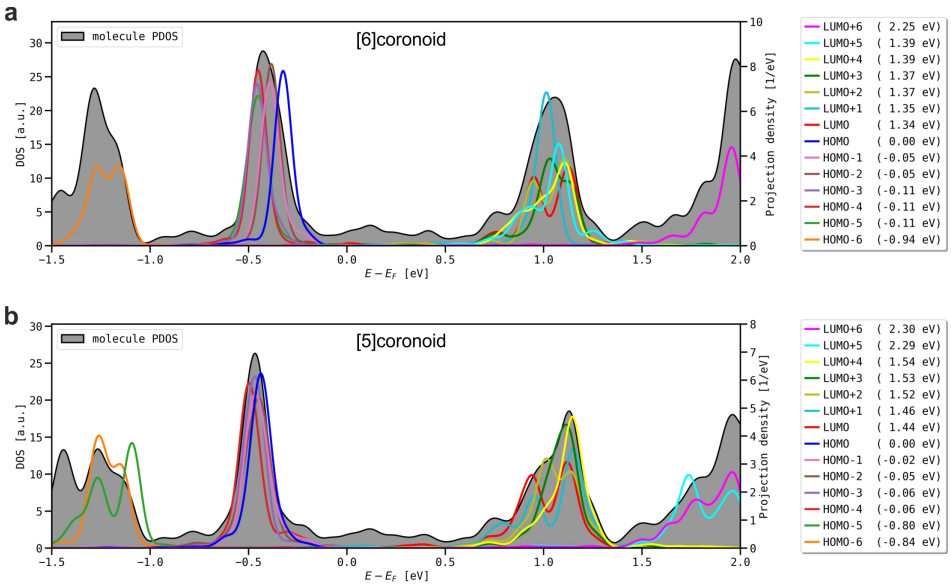

Figure S4. DFT (PBE) projected density of states (PDOS) analysis of the [6]- and [5]coronoids adsorbed on Au(111) (filled grey line) together with state projection to orbitals of the isolated (gas phase) molecules in their adsorption conformation (colored lines). Fermi energy is taken to be zero. Orbital energies of the isolated molecules are given in the legend with the HOMO energy taken as zero. (a) [6]coronoid PDOS analysis. (b) [5]coronoid PDOS analysis. All calculated states were broadened with a Gaussian of 0.10 eV full width at half maximum.

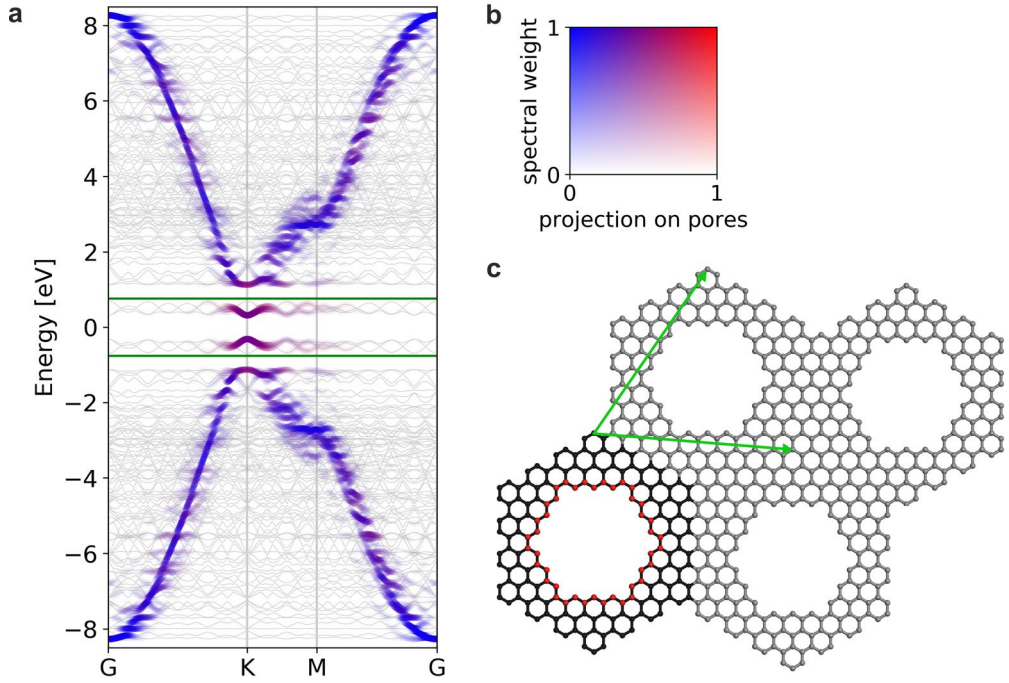

Figure S5. Tight-binding (TB) band structure of porous graphene built up from [6]coronoids. (a) Spectral weight analysis[20,21] of the porous graphene band structure unfolded to the Brillouin zone of pristine graphene. Light gray bands show the folded band structure without spectral weight analysis. The opacity of the data points (blue or red) corresponds to the magnitude of their spectral weights, resulting in the effective band structure, which illustrates the effect of the pores on the band structure of pristine graphene. Red color shows the projection of the electronic states to the atoms in proximity of the pore, as highlighted in (c). Green horizontal lines show the TB HOMO and LUMO orbital energies (–0.75 and 0.75 eV) for an isolated [6]coronoid. The band gap of this extended porous graphene layer is 0.63 eV. (b) Color map used in the band structure plot. (c) Geometry of the porous graphene. Four unit cells are shown. Green arrows indicate the lattice vectors. All atoms shown are carbon, with red ones representing those in proximity of the pore, used in the projection analysis. Tight binding calculations were performed with a nearest neighbor model of p_z orbitals of carbon with a hopping integral of t=–2.8 eV. Fermi energy is taken to be zero.

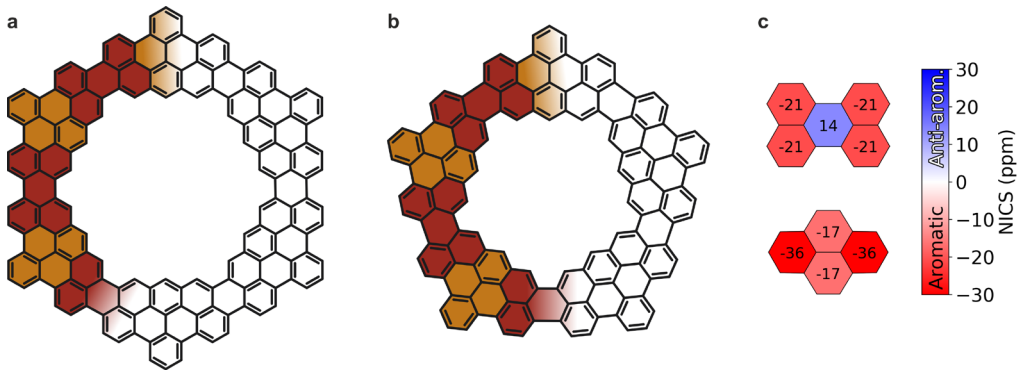

Figure S6. (a,b) The [6]- and [5]coronoid can be seen as consisting of fused perylene (brown) and pyrene (dark yellow) moieties. (c) $NICS_{zz}(1)$ patterns of these two molecules.

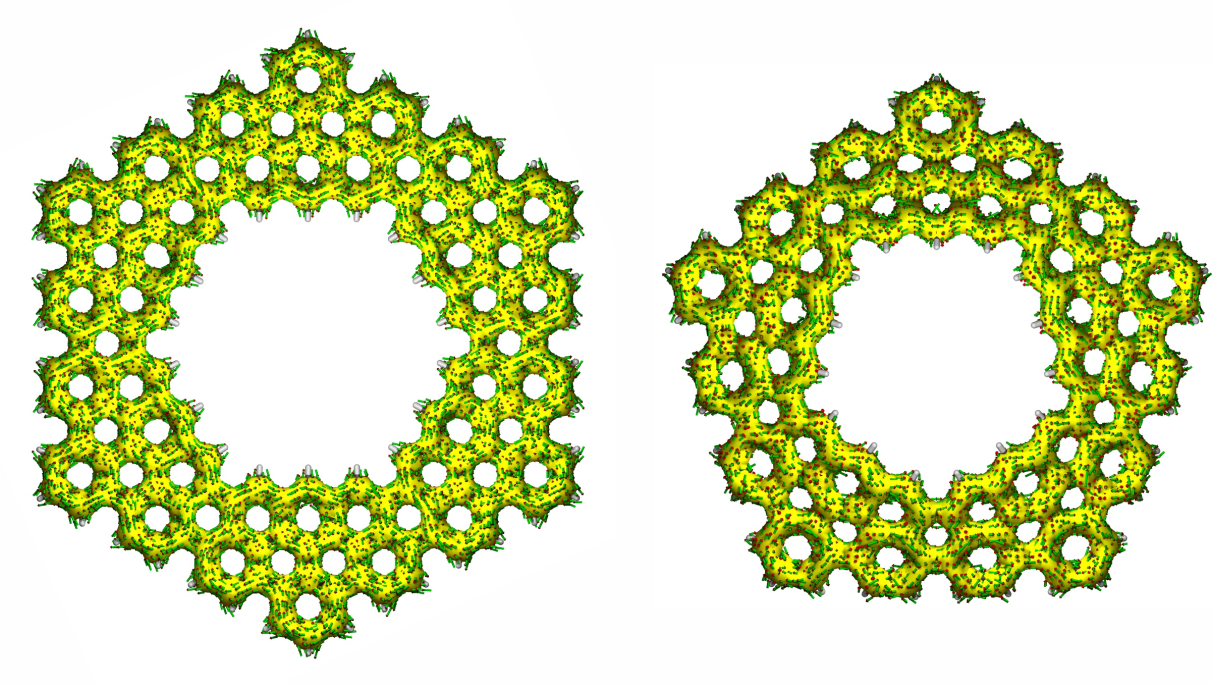

Figure S7. Magnified ACID plots (from Figure 4c,f in the main text).

NMR and mass spectra

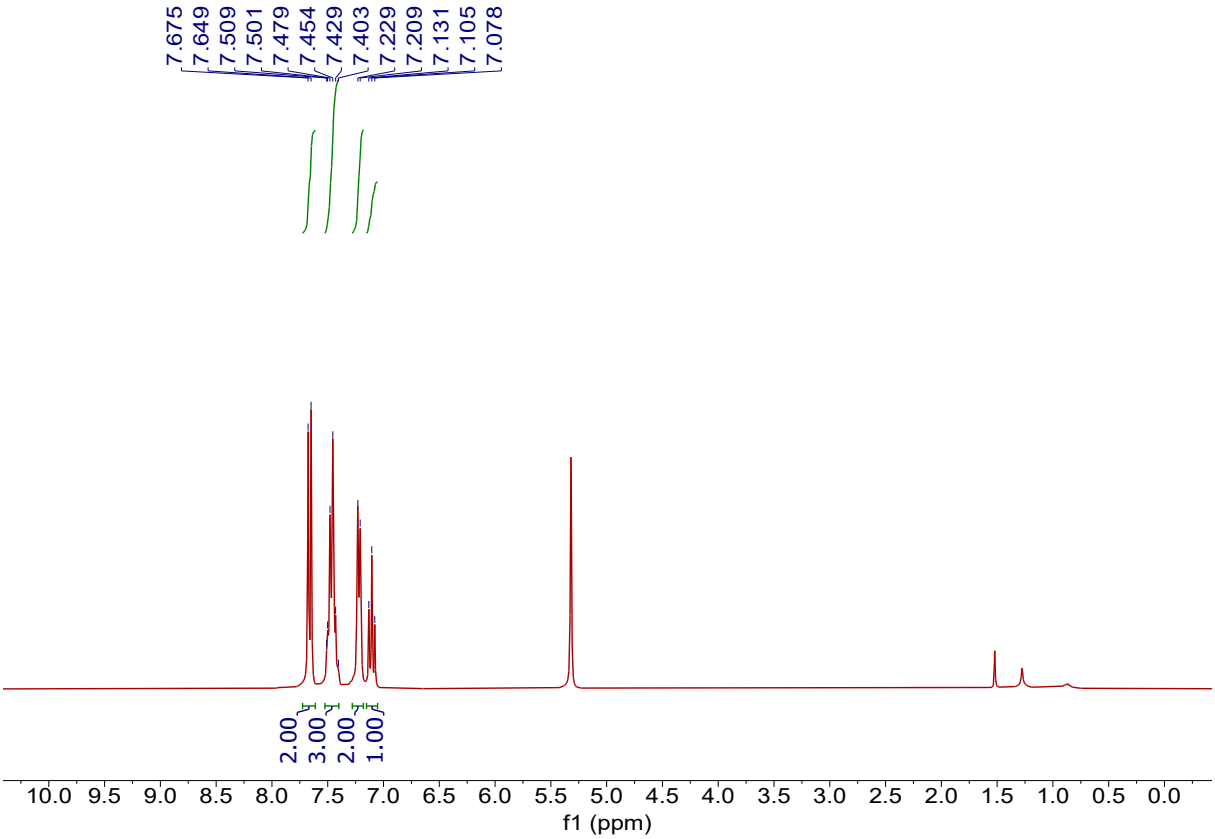

Figure S8. ^{1}H NMR spectrum of **3** (300 MHz, CD_2Cl_2, 298 K).

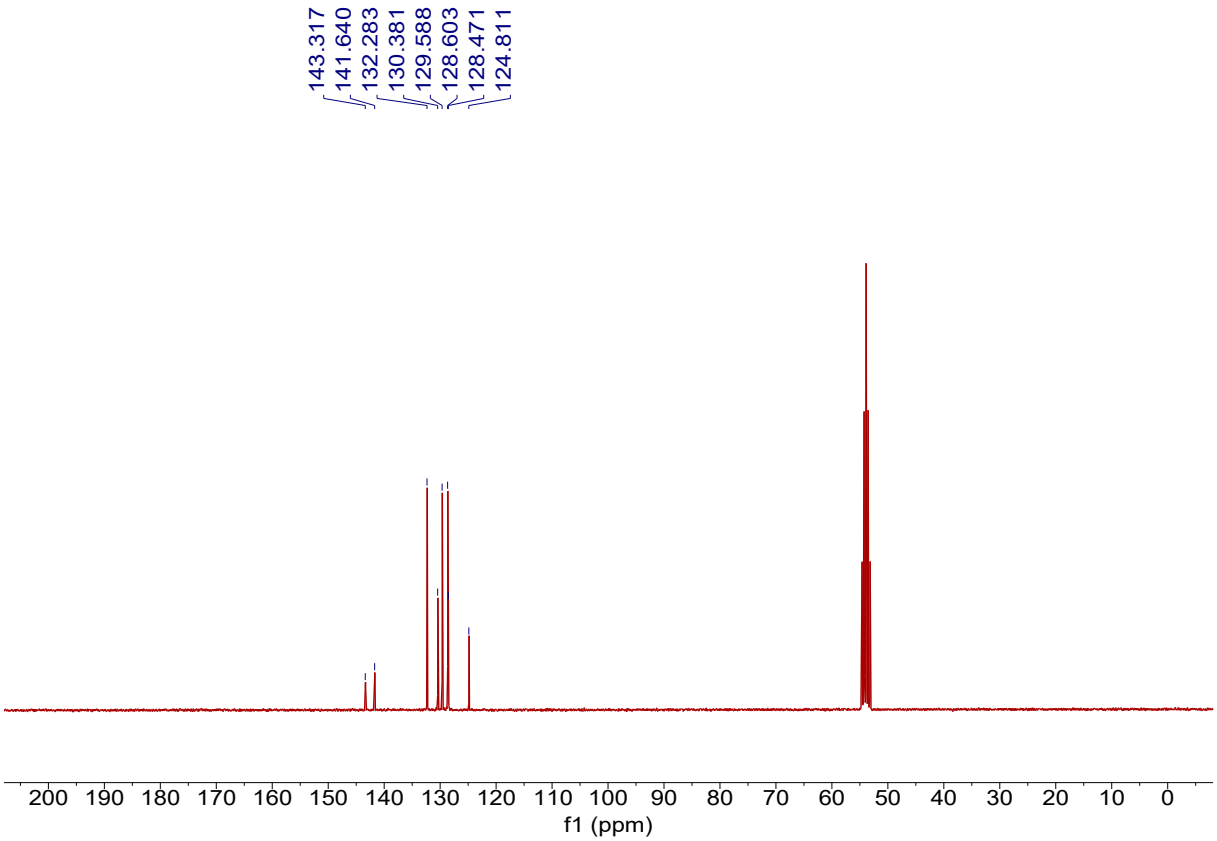

Figure S9. ^{13}C NMR spectrum of **3** (75 MHz, CD_2Cl_2, 298 K).

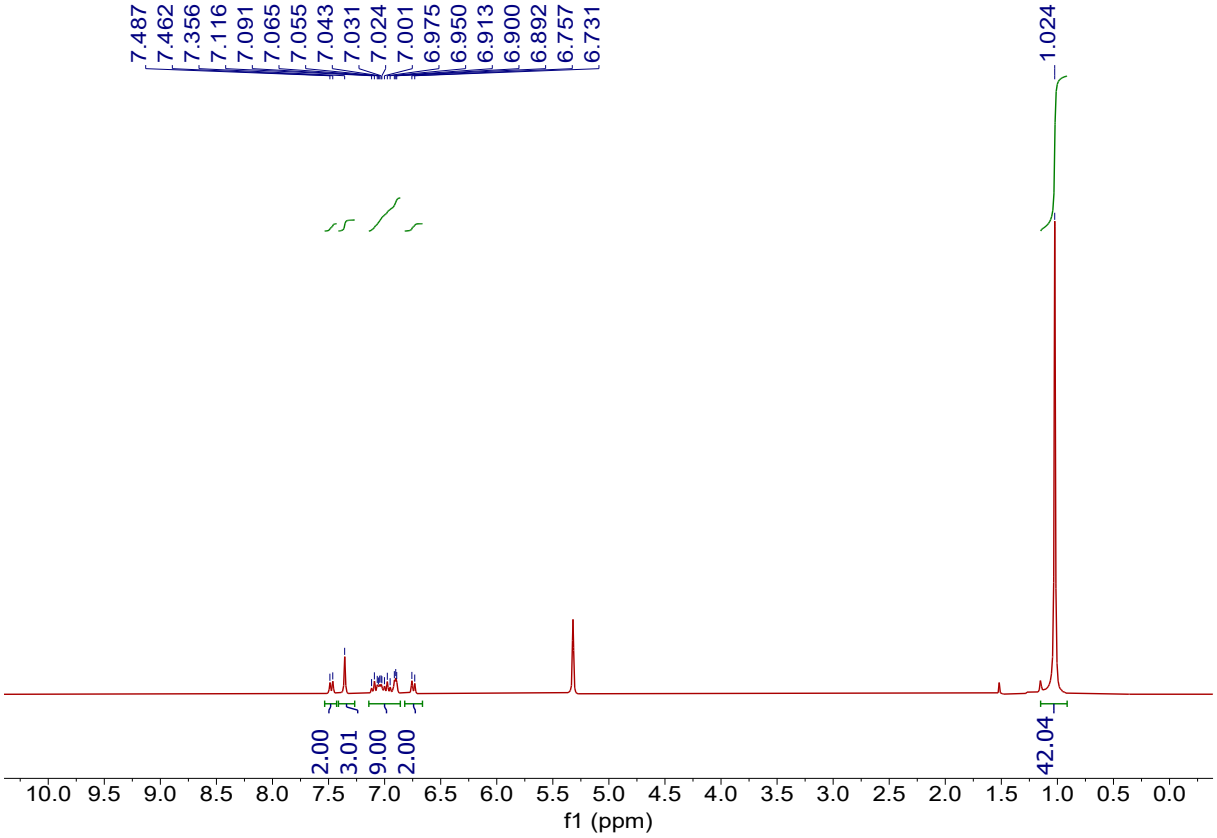

Figure S10. ^{1}H NMR spectrum of **5** (300 MHz, CD_2Cl_2, 298 K).

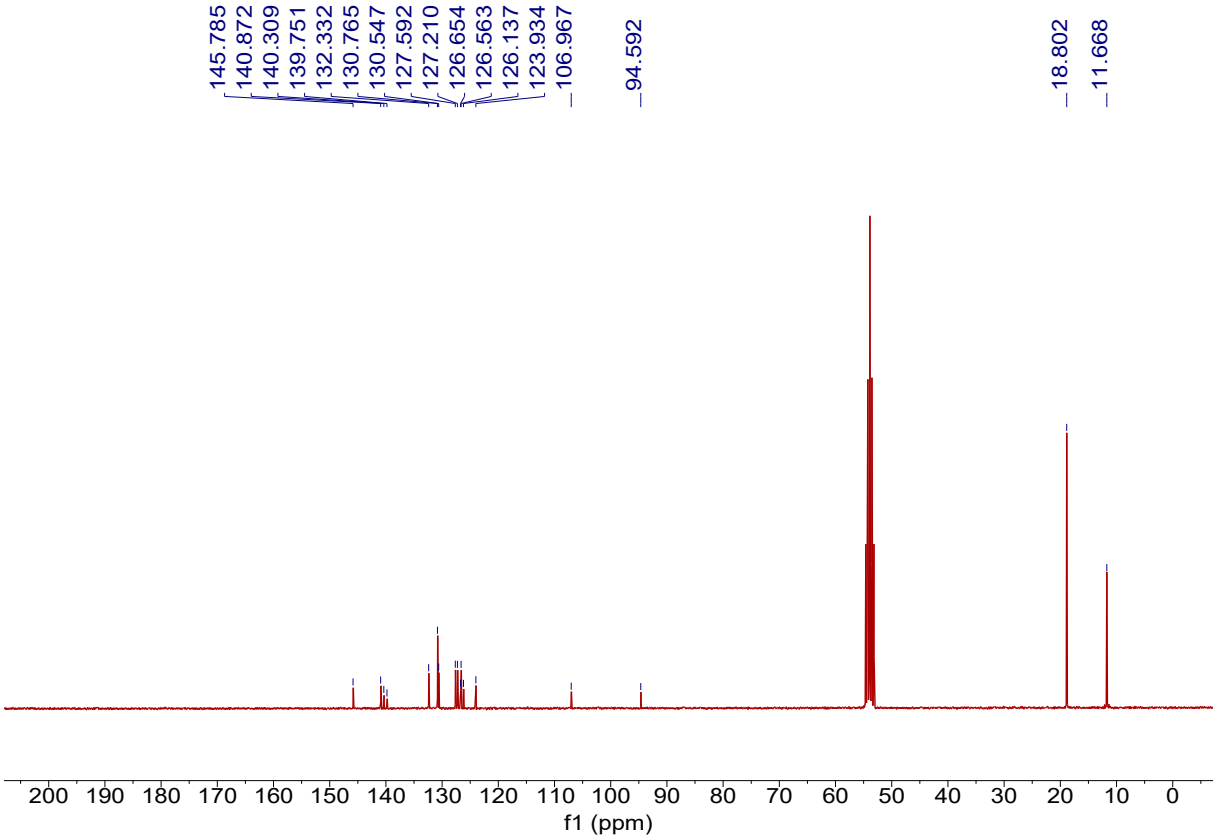

Figure S11. ^{13}C NMR spectrum of **5** (75 MHz, CD_2Cl_2, 298 K).

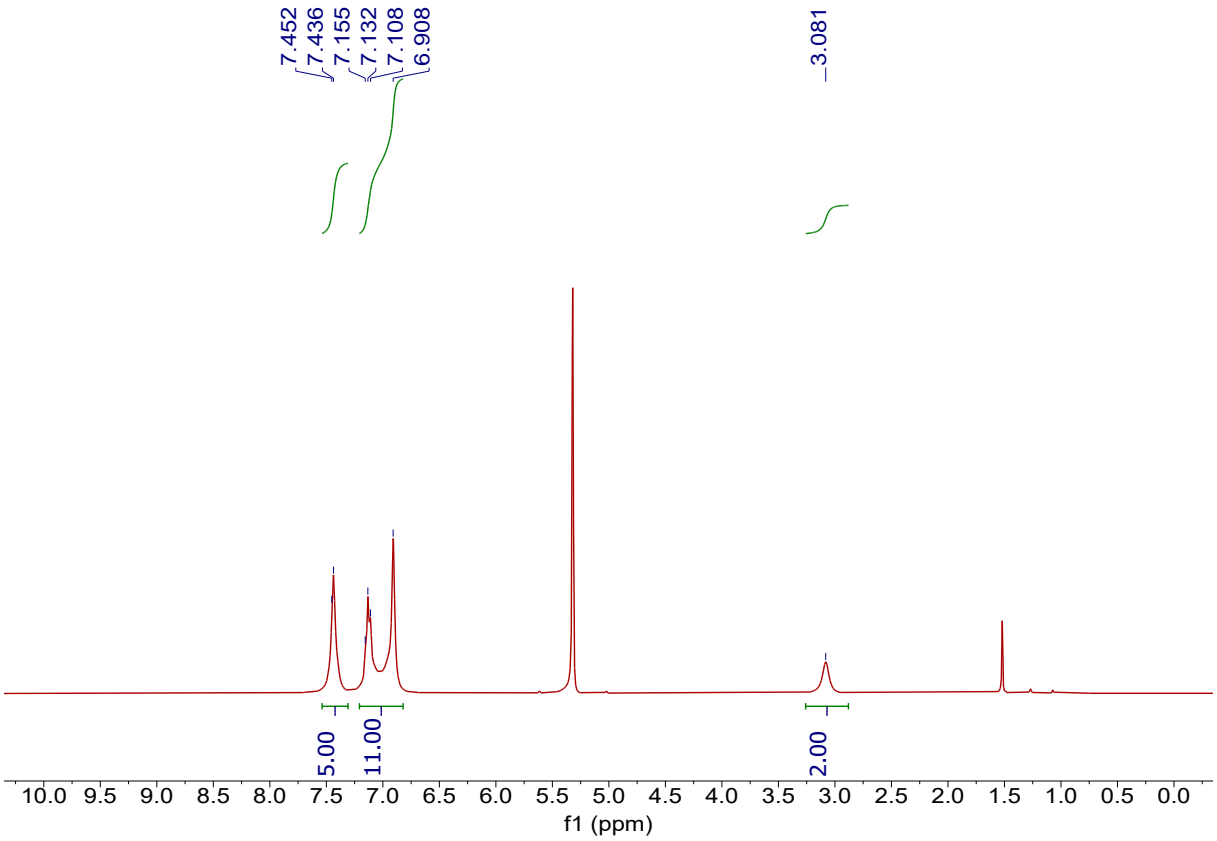

Figure S12. ^{1}H NMR spectrum of **6** (300 MHz, CD_2Cl_2, 298 K).

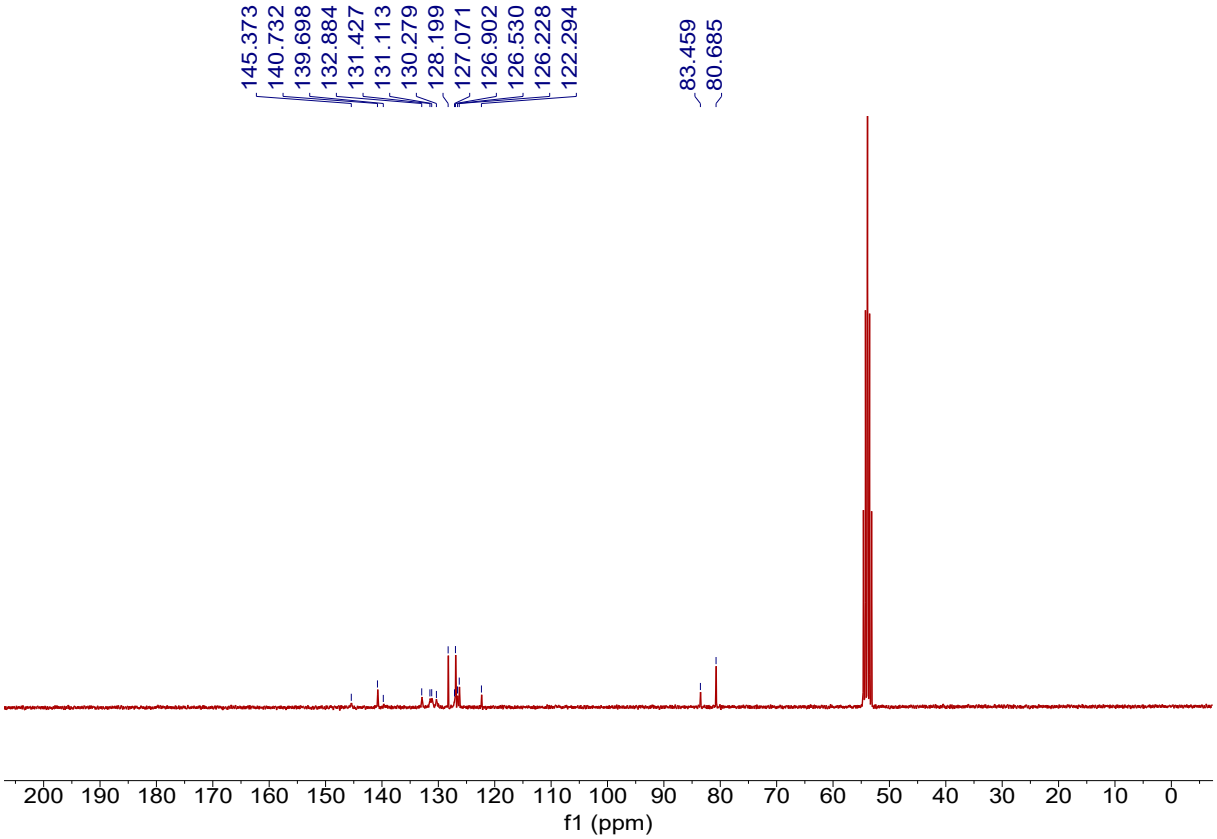

Figure S13. ^{13}C NMR spectrum of **6** (75 MHz, CD_2Cl_2, 298 K).

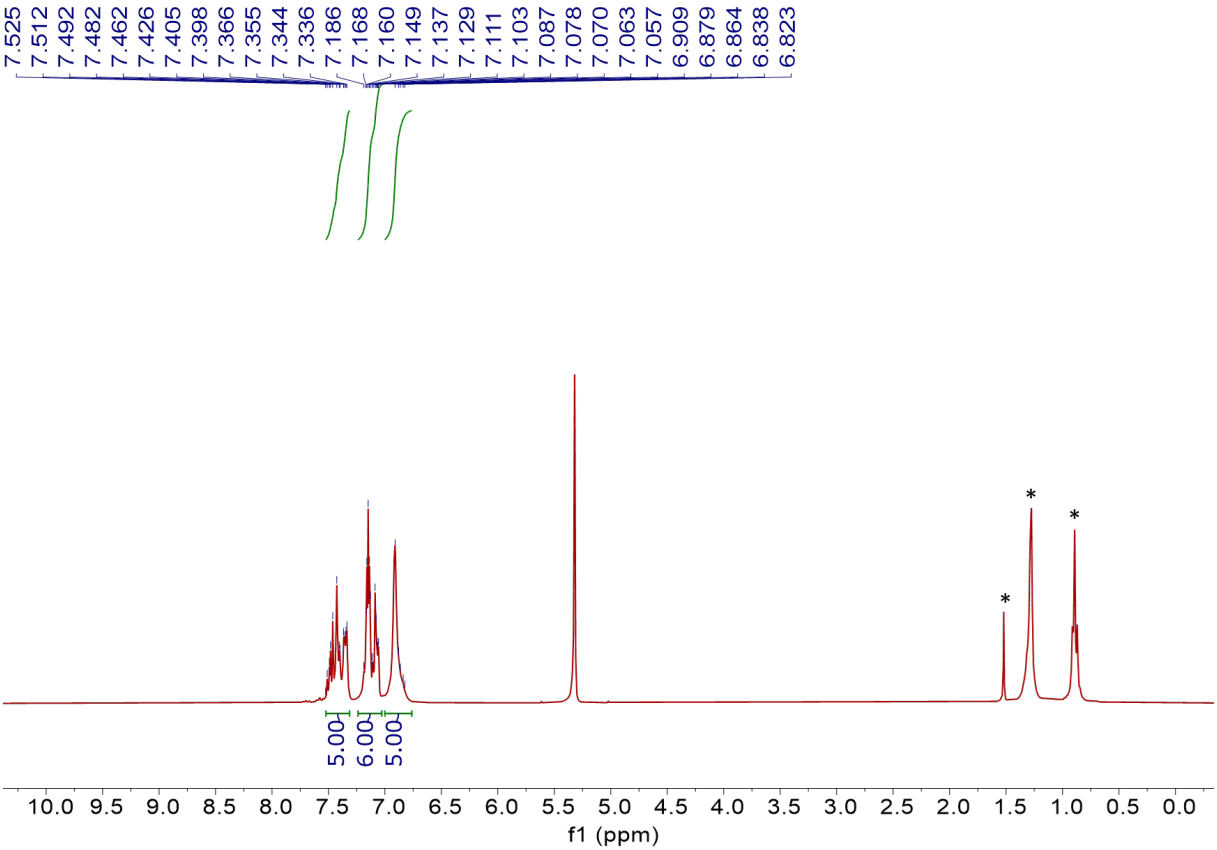

Figure S14. ^{1}H NMR spectrum of **7** (300 MHz, CD_2Cl_2, 298 K). Asterisks indicate the signal from water and *n*-hexane.

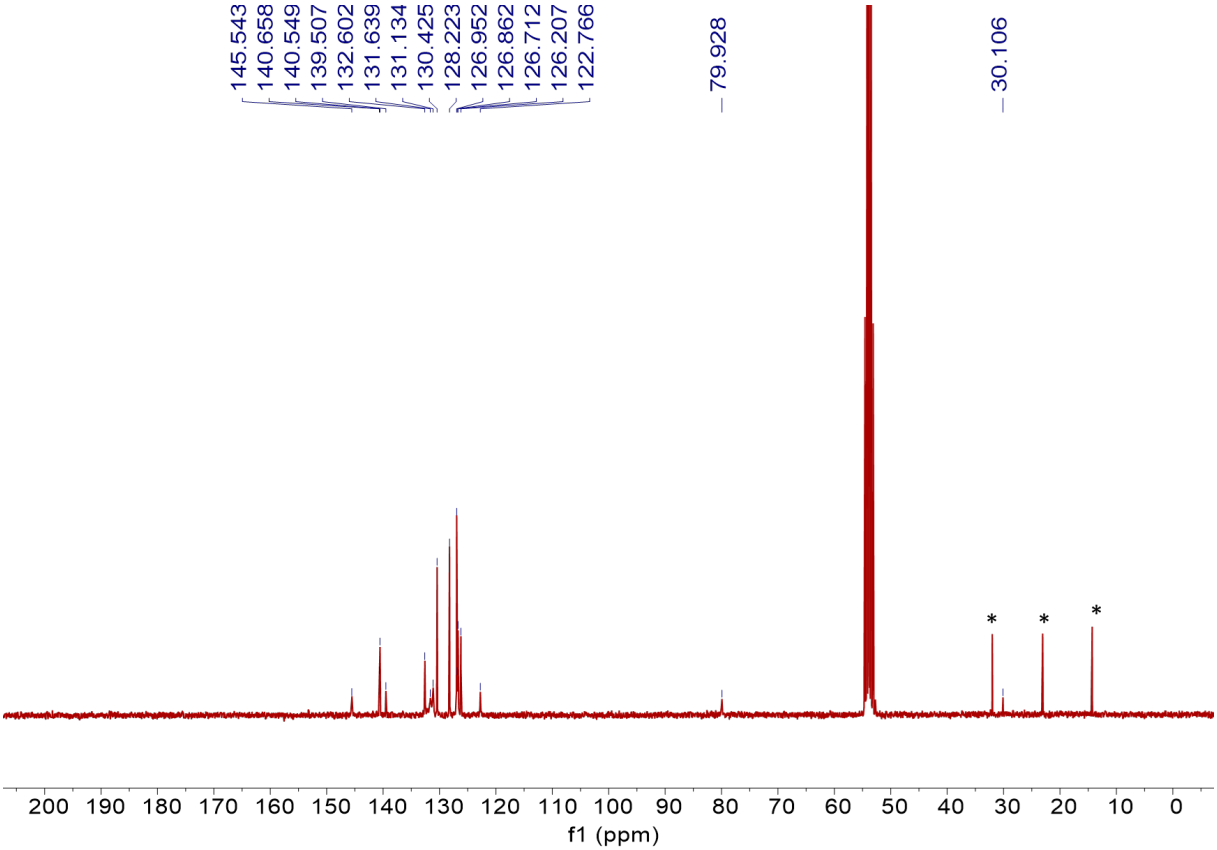

Figure S15. ^{13}C NMR spectrum of **7** (75 MHz, CD_2Cl_2, 298 K). Asterisks indicate the signal from *n*-hexane.

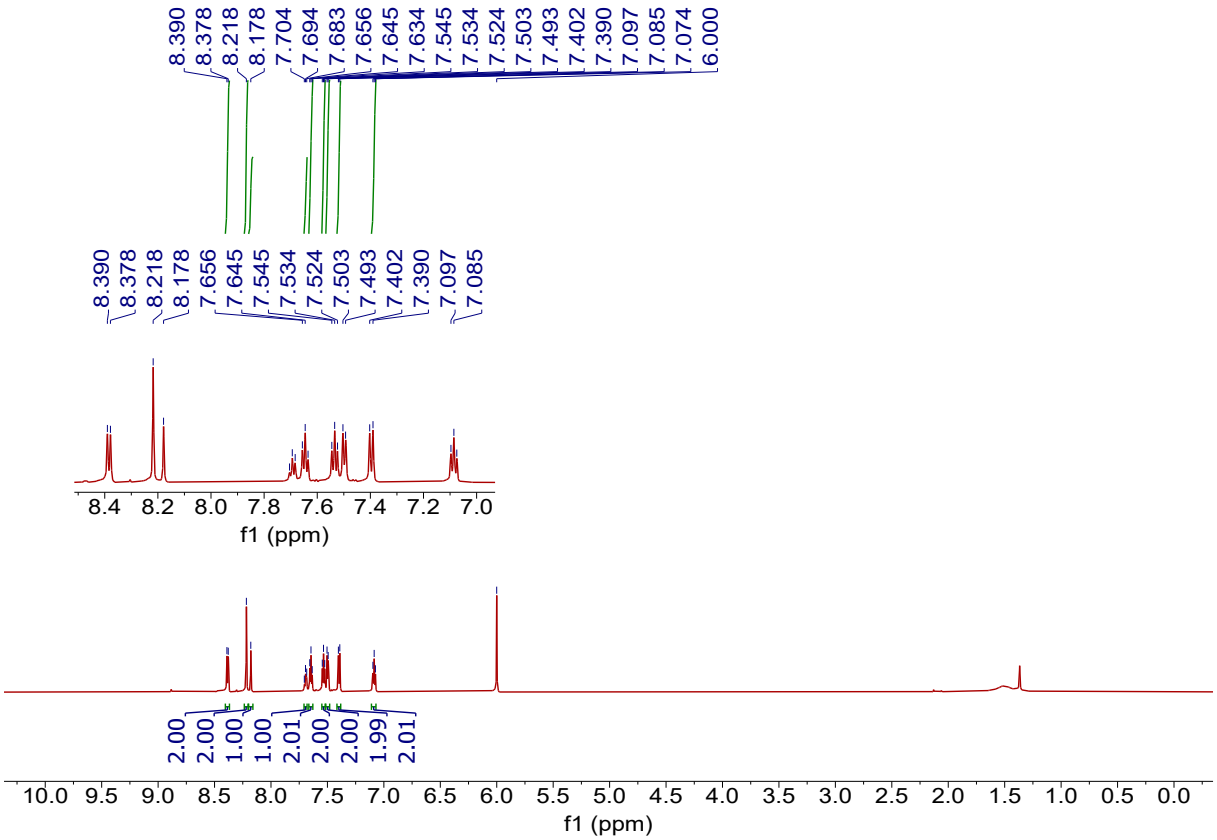

Figure S16. ^{1}H NMR spectrum of **1** (700 MHz, $C_2D_2Cl_4$, 393 K).

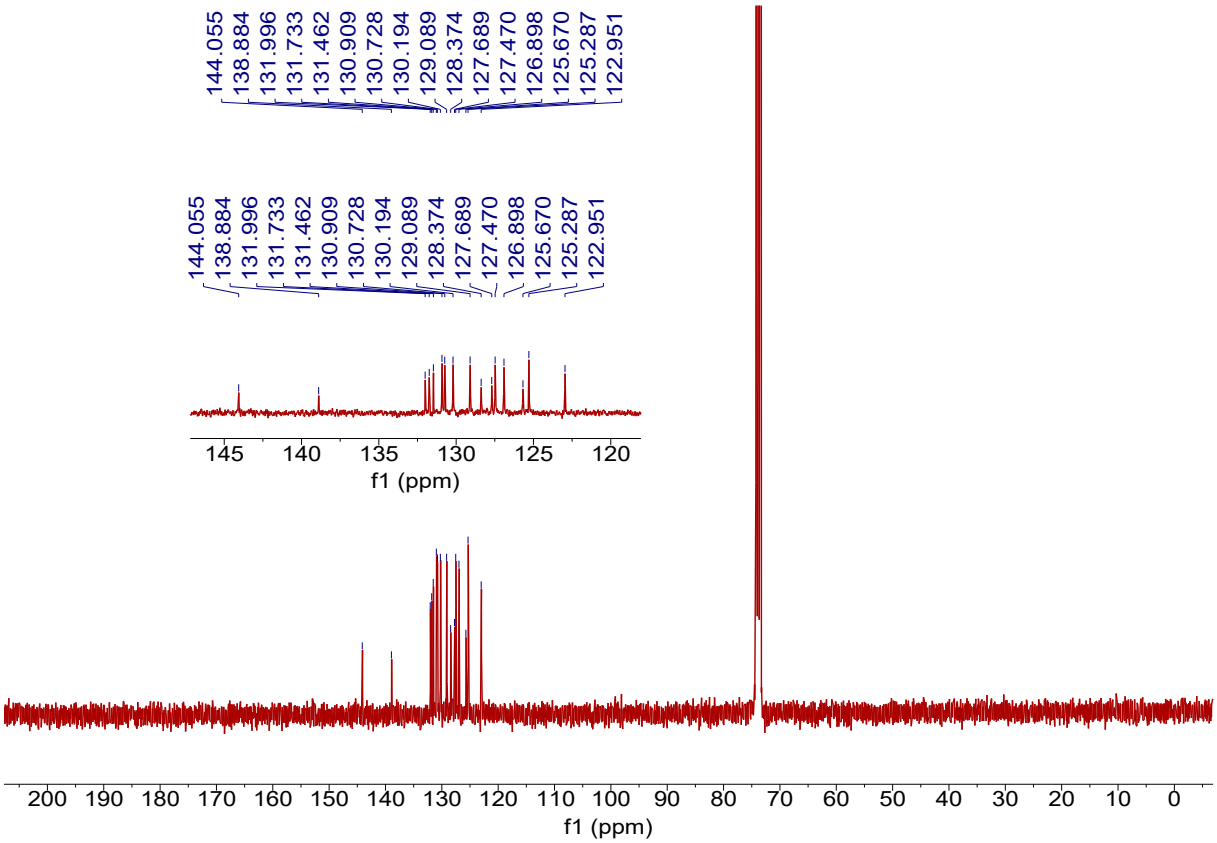

Figure S17. ^{13}C NMR spectrum of **1** (75 MHz, $C_2D_2Cl_4$, 298 K).

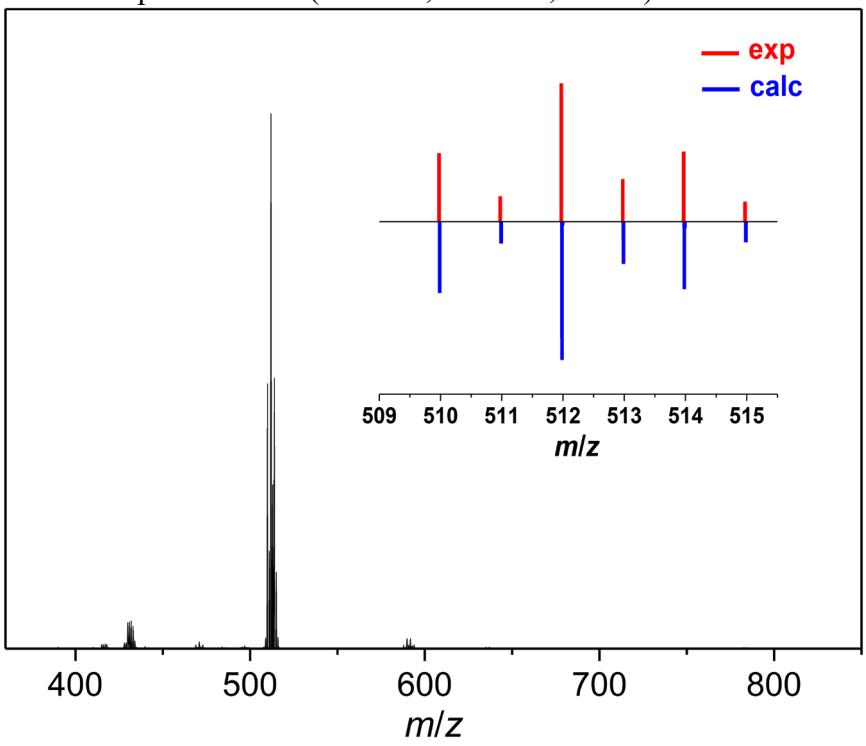

Figure S18. High-resolution MALDI-TOF mass spectrum of precursor **1**. Inset display the isotopic distribution in comparison to the calculated pattern.

References

(1) Giessibl, F. J. Atomic Resolution on Si(111)-(7×7) by Noncontact Atomic Force Microscopy with a Force Sensor Based on a Quartz Tuning Fork. *Appl Phys Lett* **2000**, *76* (11), 1470–1472.

(2) Bartels, L.; Meyer, G.; Rieder, K.-H.; Velic, D.; Knoesel, E.; Hotzel, A.; Wolf, M.; Ertl, G. Dynamics of Electron-Induced Manipulation of Individual CO Molecules on Cu(111). *Phys. Rev. Lett.* **1998**, *80* (9), 2004–2007.

(3) Hutter, J.; Iannuzzi, M.; Schiffmann, F.; VandeVondele, J. Cp2k: Atomistic Simulations of Condensed Matter Systems. *Wiley Interdiscip. Rev. Comput. Mol. Sci.* **2014**, *4* (1), 15–25.

(4) Pizzi, G.; Cepellotti, A.; Sabatini, R.; Marzari, N.; Kozinsky, B. AiiDA: Automated Interactive Infrastructure and Database for Computational Science. *Comput. Mater. Sci.* **2016**, *111*, 218–230.

(5) VandeVondele, J.; Hutter, J. Gaussian Basis Sets for Accurate Calculations on Molecular Systems in Gas and Condensed Phases. *J. Chem. Phys.* **2007**, *127* (11), 114105.

(6) Goedecker, S.; Teter, M.; Hutter, J. Separable Dual-Space Gaussian Pseudopotentials. *Phys. Rev. B* **1996**, *54* (3), 1703–1710.

(7) Perdew, J. P.; Burke, K.; Ernzerhof, M. Generalized Gradient Approximation Made Simple. *Phys. Rev. Lett.* **1996**, *77* (18), 3865–3868.

(8) Grimme, S.; Antony, J.; Ehrlich, S.; Krieg, H. A Consistent and Accurate Ab Initio Parametrization of Density Functional Dispersion Correction (DFT-D) for the 94 Elements H-Pu. *J. Chem. Phys.* **2010**, *132* (15), 154104.

(9) Tersoff, J. D.; Hamann, D. R. Theory of the Scanning Tunneling Microscope. *Phys. Rev. B* **1985**, *31* (2), 805–813.

(10) Hapala, P.; Kichin, G.; Wagner, C.; Tautz, F. S.; Temirov, R.; Jelínek, P. Mechanism of High-Resolution STM/AFM Imaging with Functionalized Tips. *Phys. Rev. B* **2014**, *90* (8), 085421.

(11) Yakutovich, A. V. Theoretical Characterization of Organic Molecules on Metallic Surfaces: Adsorption, Assembly, Chirality. PhD Thesis, University of Zürich: Zürich, 2018.

(12) Bayly, C. I.; Cieplak, P.; Cornell, W.; Kollman, P. A. A Well-Behaved Electrostatic Potential Based Method Using Charge Restraints for Deriving Atomic Charges: The RESP Model. *J. Phys. Chem.* **1993**, *97* (40), 10269–10280.

(13) Frisch, M. J.; Trucks, G. W.; Schlegel, H. B.; Scuseria, G. E.; Robb, M. A.; Cheeseman, J. R.; Scalmani, G.; Barone, V.; Mennucci, B.; Petersson, G. A.; Nakatsuji, H.; Caricato, M.; Li, X.; Hratchian, H. P.; Izmaylov, A. F.; Bloino, J.; Zheng, G.; Sonnenberg, J. L.; Hada, M.; Ehara, M.; Toyota, K.; Fukuda, R.; Hasegawa, J.; Ishida, M.; Nakajima, T.; Honda, Y.; Kitao, O.; Nakai, H.; Vreven, T.; Montgomery Jr., J. A.; Peralta, J. E.; Ogliaro, F.; Bearpark, M. J.; Heyd, J.; Brothers, E. N.; Kudin, K. N.; Staroverov, V. N.; Kobayashi, R.; Normand, J.; Raghavachari, K.; Rendell, A. P.; Burant, J. C.; Iyengar, S. S.; Tomasi, J.; Cossi, M.; Rega, N.; Millam, N. J.; Klene, M.; Knox, J. E.; Cross, J. B.; Bakken, V.; Adamo, C.; Jaramillo, J.; Gomperts, R.; Stratmann, R. E.; Yazyev, O.; Austin, A. J.; Cammi, R.; Pomelli, C.; Ochterski, J. W.; Martin, R. L.; Morokuma, K.; Zakrzewski, V. G.; Voth, G. A.; Salvador, P.; Dannenberg, J. J.; Dapprich, S.; Daniels, A. D.; Farkas, Ã.; Foresman, J. B.; Ortiz, J. V.; Cioslowski, J.; Fox, D. J. *Gaussian 09*; Gaussian, Inc.: Wallingford, CT, USA, 2016.

(14) Gershoni-Poranne, R.; Stanger, A. The NICS-XY-Scan: Identification of Local and Global Ring Currents in Multi-Ring Systems. *Chem. – Eur. J.* **2014**, *20* (19), 5673–5688.

(15) Herges, R.; Geuenich, D. Delocalization of Electrons in Molecules. *J. Phys. Chem. A* **2001**, *105* (13), 3214–3220.

(16) Geuenich, D.; Hess, K.; Köhler, F.; Herges, R. Anisotropy of the Induced Current Density (ACID), a General Method To Quantify and Visualize Electronic Delocalization. *Chem. Rev.* **2005**, *105* (10), 3758–3772.

(17) Keith, T. A.; Bader, R. F. W. Calculation of Magnetic Response Properties Using a Continuous Set of Gauge Transformations. *Chem. Phys. Lett.* **1993**, *210* (1), 223–231.

(18) Leroux, F. R.; Berthelot, A.; Bonnafoux, L.; Panossian, A.; Colobert, F. Transition-Metal-Free Atropo-Selective Synthesis of Biaryl Compounds Based on Arynes. *Chem. – Eur. J.* **2012**, *18* (45), 14232–14236.

(19) Felber, B.; Diederich, F. Synthesis of Dendritic Metalloporphyrins with Distal H-Bond Donors as Model Systems for Hemoglobin. *Helv. Chim. Acta* **2005**, *88* (1), 120–153.

(20) Popescu, V.; Zunger, A. Extracting E versus k Effective Band Structure from Supercell Calculations on Alloys and Impurities. *Phys. Rev. B* **2012**, *85* (8), 085201.

(21) Lee, C.-C.; Yamada-Takamura, Y.; Ozaki, T. Unfolding Method for First-Principles LCAO Electronic Structure Calculations. *J. Phys. Condens. Matter* **2013**, *25* (34), 345501.